Monthly Notices
of the
ROYAL ASTRONOMICAL SOCIETY

MNRAS **477,** 741–754 (2018) doi:10.1093/mnras/sty672
Advance Access publication 2018 March 14

Gravitational corrections to light propagation in a perturbed FLRW universe and corresponding weak-lensing spectra

Carolina Cuesta-Lazaro, Arnau Quera-Bofarull, Robert Reischke and Björn Malte Schäfer★

Astronomisches Rechen-Institut, Zentrum für Astronomie der Universität Heidelberg, Philosophenweg 12, D-69120 Heidelberg, Germany

Accepted 2018 March 9. Received 2018 March 7; in original form 2017 December 23

ABSTRACT

When the gravitational lensing of the large-scale structure is calculated from a cosmological model a few assumptions enter: (i) one assumes that the photons follow unperturbed background geodesics, which is usually referred to as the Born approximation, (ii) the lenses move slowly, (iii) the source-redshift distribution is evaluated relative to the background quantities, and (iv) the lensing effect is linear in the gravitational potential. Even though these approximations are small individually they could sum up, especially since they include local effects such as the Sachs–Wolfe and peculiar motion, but also non-local ones like the Born approximation and the integrated Sachs–Wolfe effect. In this work, we will address all points mentioned and perturbatively calculate the effect on a tomographic cosmic shear power spectrum of each effect individually as well as all cross-correlations. Our findings show that each effect is at least 4–5 orders of magnitude below the leading order lensing signal. Finally, we sum up all effects to estimate the overall impact on parameter estimation by a future cosmological weak-lensing survey such as *Euclid* in a *w*cold dark matter cosmology with parametrization Ω_m, σ_8, n_s, h, w_0, and w_a, using five tomographic bins. We consistently find a parameter bias of 10^{-5}, which is therefore completely negligible for all practical purposes, confirming that other effects such as intrinsic alignments, magnification bias and uncertainties in the redshift distribution will be the dominant systematic source in future surveys.

Key words: gravitational lensing: weak – dark energy – large-scale structure of Universe.

1 INTRODUCTION

Measuring weak gravitational lensing of the large-scale structure (LSS, Bacon, Refregier & Ellis 2000; Van Waerbeke et al. 2000; Kaiser, Wilson & Luppino 2001; Amara & Réfrégier 2007; Hoekstra & Jain 2008; Kilbinger et al. 2009; Kayo, Takada & Jain 2013; Kitching et al. 2014; Kilbinger 2015), called cosmic shear, is a key scientific goal in upcoming cosmological surveys such as *Euclid* (Laureijs et al. 2011) or the *Large Synoptic Survey Telescope* (LSST, LSST Science Collaboration et al. 2009). These surveys will provide data over a vast range of scales. In particular, they will probe the small scales with unrivalled precision enabling to measure the cosmic shear signal at roughly 1000σ significance. Measuring the weak-lensing signal at such a high significance is a challenge on its own (see e.g. Bridle 2010; Miller et al. 2013; Croft et al. 2017; Hoekstra, Viola & Herbonnet 2017), but also on the theoretical side quite a few systematics exists, most notably intrinsic alignments of galaxies, which can mimic a weak-lensing signal (e.g. Croft & Metzler 2000; Lee 2011; Joachimi et al. 2015; Blazek, Vlah & Seljak 2015; Schaefer & Merkel 2017).

To infer, in the very end, cosmological parameters from cosmic shear measurements the lensing signal must be calculated from a cosmological model and include all effects present in the observation. Otherwise systematic effects in the inference process can occur (Amara & Réfrégier 2008). The cosmic shear signal is usually given in tomographic bins to restore redshift information (Hu 1999; Takada & White 2004; Amara & Réfrégier 2007) or in a spherical basis using spherical Bessel functions (Heavens 2003; Castro, Heavens & Kitching 2005). Furthermore, the lensing potential is calculated in a weakly perturbed space–time relative to a Friedmann–Lemaître–Robertson–Walker (FLRW) by tracing null geodesics by virtue of the Jacobi equation, describing how a bundle of light rays is deformed along their path. The equation of geodesic deviation is then sourced by gradients in the Newtonian potential, Φ, or in presence of anisotropic stress by the difference

★ E-mail: bjoern.malte.schaefer@uni-heidelberg.de

of the two Bardeen Potentials. Since $\Phi \ll c^2$, deflection angles are small and the integration is usually carried out along unperturbed rays, this is known as the Born approximation, which is satisfied very well as shown by different numerical simulations (Jain, Seljak & White 2000; Dodelson et al. 2005; Shapiro & Cooray 2006; Hilbert et al. 2009). A second-order treatment can also be found in Cooray & Hu (2002) and Bernardeau, Bonvin & Vernizzi (2010). Peculiar velocity effects have been discussed in Bonvin (2008), while other systematic effects such as multiple deflections have been treated in Seitz & Schneider (1994) and Krause & Hirata (2010).

The statistical properties of the lensing potential of the LSSs are then expressed in terms of angular correlation function in a suitable basis (Hu 1999; Heavens 2003; Schäfer & Heisenberg 2012; Kitching et al. 2017). At its heart, it involves a line-of-sight projection of the power spectrum of the potential fluctuations, or equivalently of the matter power spectrum. Cosmological information is mainly contained in the lensing kernel and especially in the distance redshift relation. As described before, the natural coordinate choice for weak cosmological lensing are comoving coordinates together with conformal time, however only the redshift z is observable, which has to be related to the comoving distance χ. In calculating the cosmic shear power spectrum, one thus assumes sources measured at redshift z to be at unperturbed comoving distances χ. However, redshift space distortions (e.g. Percival et al. 2011) add an additional contribution to the cosmological redshift. The observed redshift distributions does therefore not correspond to the ideally assumed one used for the calculation of the cosmic shear power spectrum. Furthermore, the Born approximation results into a temporal and spatial part. The effect of the temporal Born correction changes the evolutionary state at which a photon passes cosmic structures and therefore the lensing signal is changed. Other effects involve the kinetic contributions of the LSS to the lensing potential. In this paper, we calculate the magnitude of those effects, particularly we investigate redshift space distortions, second-order correction to the effective refraction index, the temporal Born approximation, Sachs–Wolfe effects, and gravitomagnetic effects. We calculate the corrections to the tomographic cosmic shear signal by calculation the contribution of the auto- and cross-correlations of the effects mentioned. The effects are compared to weak-lensing spectra as being measured by *Euclid*.

Throughout the paper, we will use a spatially flat $w$cold dark matter (wCDM) cosmology, with specific parameter choices $\Omega_\mathrm{m} = 0.25$, $n_\mathrm{s} = 1$, $\sigma_8 = 0.8$, and $h = 0.7$, and $w = -1$ for the fiducial cosmology. The structure of the paper is as follows: after a summary of cosmology in Section 2 and weak gravitational lensing in Section 3, we work out all corrections in Section 4 and evaluate them numerically in Section 5. We summarize and discuss our results in Section 6.

2 COSMOLOGY

Under the symmetry assumption of Friedmann–Lemaître cosmologies, all fluids are characterized by their density and their equation of state: In spatially, flat cosmologies with the matter density parameter Ω_m and the corresponding dark energy density $1 - \Omega_\mathrm{m}$, one obtains for the Hubble function $H(a) = \dot{a}/a$ the expression,

$$\frac{H^2(a)}{H_0^2} = \frac{\Omega_\mathrm{m}}{a^3} + \frac{1-\Omega_\mathrm{m}}{a^{3(1+w)}}, \tag{1}$$

for a constant dark energy equation of state parameter w. The comoving distance χ is related to the scale factor a through

$$\chi = -c\int_1^a \frac{\mathrm{d}a'}{a'^2 H(a')}, \tag{2}$$

where the Hubble distance $\chi_\mathrm{H} = c/H_0$ sets the distance scale for cosmological distance measures. Cosmic deceleration $q = \ddot{a}a/\dot{a}^2$ is related to the logarithmic derivative of the Hubble function, $2 - q = 3 + \mathrm{d}\ln H/\mathrm{d}\ln a$.

Small fluctuations δ in the distribution of dark matter grow, as long as they are in the linear regime $|\delta| \ll 1$, according to the growth function $D_+(a)$ (Linder & Jenkins 2003; Wang & Steinhardt 1998),

$$\frac{\mathrm{d}^2}{\mathrm{d}a^2}D_+(a) + \frac{2-q}{a}\frac{\mathrm{d}}{\mathrm{d}a}D_+(a) - \frac{3}{2a^2}\Omega_\mathrm{m}(a)D_+(a) = 0, \tag{3}$$

and their statistics is characterized by the spectrum $\langle\delta(\boldsymbol{k})\delta^*(\boldsymbol{k}')\rangle = (2\pi)^3\delta_\mathrm{D}(\boldsymbol{k}-\boldsymbol{k}')P_\delta(k)$. Inflation generates a spectrum of the form $P_\delta(k) \propto k^{n_s}T^2(k)$ with the transfer function $T(k)$ (Eisenstein & Hu 1999, 1998) which is normalized to the variance σ_8^2 smoothed to the scale of 8 Mpc h^{-1},

$$\sigma_8^2 = \int_0^\infty \frac{k^2\mathrm{d}k}{2\pi^2}\, W^2(8\,\mathrm{Mpc}\,h^{-1}\times k)\, P_\delta(k), \tag{4}$$

with a Fourier-transformed spherical top-hat $W(x) = 3j_1(x)/x$ as the filter function. From the CDM spectrum of the density perturbation, the spectrum of the Newtonian gravitational potential Φ can be obtained,

$$P_\Phi(k;\chi) = \left(\frac{3\Omega_\mathrm{m}H_0^2}{2}\right)^2 k^{-4}P_\delta(k;\chi) \propto \left(\frac{3\Omega_\mathrm{m}H_0^2}{2}\right)^2 k^{n_s-4}\,T(k)^2, \tag{5}$$

by applying the comoving Poisson equation $\Delta\Phi = \frac{3\Omega_\mathrm{m}H_0^2}{2}\delta$ for deriving the gravitational potential Φ from the density δ. With equation (3) yielding a solution for the homogeneous growth of the density contrast. It should be noted that velocities at linear order are obtained from the continuity equation,

$$\boldsymbol{\nabla}\cdot\boldsymbol{v} = -a\dot{\delta}, \tag{6}$$

such that in Fourier space,

$$\boldsymbol{v}_{\rm k} = aH(a)\frac{{\rm d}\ln(D_+)}{{\rm d}\ln(a)}\frac{\boldsymbol{k}}{k^2}\delta_{\rm k}. \tag{7}$$

3 BASICS OF COSMOLOGICAL WEAK GRAVITATIONAL LENSING

In weak gravitational lensing, one investigates the action of gravitational tidal fields on the shape of distant galaxies by the distortion of light bundles (for reviews, please refer to Bartelmann & Schneider 2001; Hoekstra & Jain 2008; Huterer 2010; Bartelmann 2010; Kilbinger 2015).

The lensing potential ψ is given by a projection integral,

$$\psi(\boldsymbol{n}, \chi) = \frac{2}{c^2}\int_0^\chi {\rm d}\chi'\, g(\chi, \chi')\Phi(\boldsymbol{n}\chi'; \chi'), \tag{8}$$

relating ψ to the gravitational potential Φ through weighting function $g(\chi, \chi')$,

$$g(\chi, \chi') = \frac{\chi' - \chi}{\chi'\chi} \tag{9}$$

with $\boldsymbol{n}$ representing the position of the lens on the sky and χ its comoving distance. Since the intrinsic ellipticities of the galaxies are unknown, but assumed to be randomly ordered, it is convenient to average the lensing potential over a source distribution $p(z)$.

$$\overline{\psi}(\boldsymbol{n}) = \int_0^{\chi_H} {\rm d}\chi\; p(z)\frac{{\rm d}z}{{\rm d}\chi}\psi(\boldsymbol{n}, \chi) = \frac{2}{c^2}\int_0^{\chi_H} {\rm d}\chi \int_\chi^{\chi_H} {\rm d}\chi' g(\chi, \chi')\Phi(\boldsymbol{n}\chi; \chi), \tag{10}$$

where we included the probability distribution inside the window function,

$$g(\chi, \chi') = \frac{\chi' - \chi}{\chi\chi'}p(\chi')\frac{{\rm d}z}{{\rm d}\chi'}, \tag{11}$$

and readjusted the integration boundaries. Note that ${\rm d}z/{\rm d}\chi' = H(a(\chi'))$. As a line of sight-integrated quantity, the projected potential contains less information than the sourcing field Φ. In order to partially regain that information, one commonly divides the sample of lensed galaxies into $n_{\rm bin}$ redshift bins and computes the lensing signal for each of the bins i separately. Denoting $g_{\rm i}(\chi, \chi')$ as the restriction of $g(\chi, \chi')$ on to the bin i, one defines the tomographic lensing efficiency function $G_{\rm i}(\chi)$,

$$G_{\rm i}(\chi) = \int_0^\chi {\rm d}\chi' g_{\rm i}(\chi, \chi'). \tag{12}$$

Euclid forecasts use the parametrization of the redshift distribution $p(z){\rm d}z$,

$$p(z){\rm d}z \propto \left(\frac{z}{z_0}\right)^2 \exp\left[-\left(\frac{z}{z_0}\right)^\beta\right]{\rm d}z, \tag{13}$$

with $\beta = 3/2$ causing a slightly faster than exponential decrease at large redshifts (Laureijs et al. 2011).

Changes in the image of a distant galaxy are encoded in the second angular derivatives of the weak-lensing potential ψ: this Jacobian matrix can be decomposed into convergence and shear with the use of Pauli matrices σ_α,

$$\psi_{\rm ab} = \sum_{\alpha=0}^{3} a_\alpha\sigma^{(\alpha)} = \kappa\sigma_{\rm ab}^{(0)} + \gamma_+\sigma_{\rm ab}^{(1)} - {\rm i}\rho\sigma_{\rm ab}^{(2)} + \gamma_\times\sigma_{\rm ab}^{(3)}\,. \tag{14}$$

Since weak gravitational lensing of a single galaxy is not observable, one is interested in the statistical properties of the convergence or the shear. The Fourier transform of the tomographic convergence correlation function, the angular power spectrum, is given by

$$C_{\rm ij}^\kappa(\ell) = \frac{9\Omega_{\rm m}^2}{16\chi_{\rm H}^4}\int\frac{{\rm d}\chi}{\chi^2}\,G_{\rm i}(\chi)G_{\rm j}(\chi)P_\delta(\ell/\chi, \chi), \tag{15}$$

where we used the Limber approximation (Limber 1954) and the comoving Poisson equation (5). Note that the spectrum (15) is equal to the E-mode spectrum of the weak-lensing shear γ.

4 CORRECTIONS TO THE WEAK-LENSING SIGNAL

In this section, we will describe the effects which will lead to corrections of the weak-lensing signal. Particularly, we are looking at the effects of peculiar velocity induced redshifts, Sachs–Wolfe effects, second-order corrections to the effective speed of light, the temporal Born approximation as well as the assumption of slowly moving lenses. All corrections originate from the metric perturbations Φ, i.e. the Newtonian gravitational potential. The calculations are effectively carried out in synchronous Newtonian gauge.

4.1 Distortions of the source redshift distribution

Distance in galaxy surveys are measured indirectly via spectroscopic (Gaztañaga et al. 2012; Cunha et al. 2014) or photometric (Bolzonella, Miralles & Pelló 2000; Bender et al. 2000) redshift determinations. Mostly, a combination of both techniques is used, such that the photometric method is calibrated with the spectroscopic one. When calculating the theoretical prediction of the lensing signal in equation (15), one implicitly assumes that lensing takes places in the ideal background cosmology, expressed by the conversion of the redshift in a comoving distance. The perturbation on this background however alters the ideal cosmological redshift and the redshift distribution gets effectively distorted due to the presence of inhomogeneities. Consequently, the lensing signal will look different as in equation (15).

Quite generically, the kernel of the lensing potential can be expanded around its homogeneous value (see equation 8)

$$\psi_{\rm ab}(\boldsymbol{n}, \chi + \Delta\chi) \approx \psi_{\rm ab}(\boldsymbol{n}, \chi) + \frac{\partial \psi_{\rm ab}(\boldsymbol{n}, \chi)}{\partial \chi}\Delta\chi = \psi_{\rm ab}(\boldsymbol{n}, \chi) + \frac{\partial \psi_{\rm ab}(\boldsymbol{n}, \chi)}{\partial \chi}\frac{\partial \chi}{\partial z}\Delta z. \tag{16}$$

Here, we keep the indices a, b as bookkeeping for the derivatives. We now rewrite the latter equation by using the Leibniz rule,

$$\psi_{\rm ab}(\boldsymbol{n}, \chi) = \frac{2}{c^2}\int_0^\chi {\rm d}\chi' g(\chi', \chi) S_{\rm ab}((\boldsymbol{n}\chi; \chi), (\boldsymbol{n}\chi'; \chi')), \tag{17}$$

where we abbreviated $S_{\rm ab}$ as the sum of the first- and second-order terms:

$$S^{(1)}_{\rm ab} = \Phi_{,{\rm ab}}(\boldsymbol{n}\chi; \chi), \quad S^{R(2)}_{\rm ab} = -\frac{\chi'}{\chi(\chi - \chi')}\Phi_{,{\rm ab}}(\boldsymbol{n}\chi'; \chi')\frac{c}{H(a(\chi))}\Delta z(\chi). \tag{18}$$

Clearly, the first term recovers the usual lensing signal, while the second term accounts for a shift in redshift due to the following effects: first, the redshift changes due to the Sachs–Wolfe and the integrated Sachs–Wolfe effect (Sachs & Wolfe 1967). Secondly, it is altered by the peculiar motion of the source galaxies in the ambient LSS (Kaiser 1987; Hamilton 1998),

$$\Delta z = \Delta z_{\rm SW} + \Delta z_{\rm ISW} + \Delta z_{\rm V}. \tag{19}$$

The Sachs–Wolfe effect is the change on the emitted photon's redshift due to the gravitational potential at the source galaxy,

$$\Delta z_{\rm SW}(\chi) = \frac{\Phi(\boldsymbol{n}\chi; \chi)}{c^2}. \tag{20}$$

The integrated Sachs–Wolfe effect describes the interaction of photons with an evolving gravitational potential along their line of sight. The line-of-sight fluctuation is given by (Sachs & Wolfe 1967)

$$\Delta z_{\rm ISW}(\chi) = \frac{2}{c^3}\int_0^\chi {\rm d}\chi' \frac{\partial}{\partial \eta}\Phi(\boldsymbol{n}\chi'; \chi'), \tag{21}$$

which vanishes for matter dominated epochs, since $\Phi = {\rm const}$ in this case. Finally, we also consider the peculiar motion contribution to the observed redshift (Kaiser 1987),

$$\Delta z_{\rm V}(\chi) = \frac{\upsilon_\parallel(\chi)}{c}, \tag{22}$$

where $\upsilon_\parallel$ is the peculiar velocity component of the source galaxy along the line of sight. Here, we compute only the peculiar motion contribution to the galaxy redshift, while effects on propagation of the light bundle due to a moving source are neglected (Bonvin 2008). Because the application that we have in mind is cosmic shear with lensed galaxies that are not part of a virialized structure, we compute the velocity field, its autocorrelation and its cross-correlation with the density and potential from linear perturbation theory. To what extend the three effects outlined above can partially cancel each other or add up depends on the details of perturbation theory and on the correlation length of the different fields involved. On very small scales, however, the variance of the velocity field would not be given by correlations of the coherent gradient field of the gravitational potential but rather by the isotropic velocities typical for virialized cosmic structures. In this case, one would expect correlations as well, for instance as the Sachs–Wolfe effect would coincide with high velocity variances, but this is not the topic of our investigation.

In principle, gravitational effects identical to those which are present at the source galaxy's location are as well active at the observer's position: There, too, would be a change to the photon's redshift due to a non-zero gravitational potential due to the embedding of the observer into local structures and there would also be a non-zero velocity relative to the deflecting LSS. For the purpose of our derivations, we have assume the observer to be an ideal FLRW observer. This assumption is violated to a similar degree as the lensed galaxies are not following FLRW geodesics. The signature of non-ideal observers are deviations on large scales, however, and possible isotropy breaking effects.

4.2 Second-order corrections to the light propagation

A common approximation made in gravitational lensing is that the gravitational potentials involved are small, i.e. $\Phi \ll c^2$. Lensing is thus studied in an effective Minkowskian space–time due to the conformal invariance off null geodesics where the perturbations are linear in the

Newtonian potential. Thus, the effective speed of light is expanded up to first order. However, higher order terms affect the lensing signal (Bernardeau et al. 2010; Giblin et al. 2017; Tansella et al. 2017):

$$c' = c\sqrt{\frac{1-\frac{2\Phi}{c^2}}{1+\frac{2\Phi}{c^2}}} \approx c - \frac{2\Phi}{c} + \frac{2\Phi^2}{c^3}\,. \tag{23}$$

The second-order term generates also second-order correction to the lensing potential, $S_{\rm ab}^{P(2)}$, that gets ultimately summed up with (18),

$$S_{\rm ab}^{P(2)} = -\frac{1}{c^2}\Phi^2_{,\rm ab}\,. \tag{24}$$

4.3 Temporal Born effect

The Born approximation sets the photon path to be an idealized straight FLRW geodesic (Schneider & Weiss 1988; Lee & Paczynski 1990; Bartelmann & Schneider 2001). Using the actual geodesics of the photons complicate matters significantly, since new positions must be computed from past deflected ones (Petri, Haiman & May 2017). This spatial aspect of the Born approximation has been widely studied before analytically (Cooray & Hu 2002; Shapiro & Cooray 2006; Krause & Hirata 2010; Schäfer et al. 2012; Petri et al. 2017) or in numerical simulations (Hilbert et al. 2009; Giblin et al. 2017), and fond to be small.

Similarly, the case of lensing of the cosmic microwave background has been treated analytically (Hagstotz, Schaefer & Merkel 2015; Pratten & Lewis 2016; Marozzi et al. 2016) and through simulations (Carbone et al. 2009; Calabrese et al. 2015), with the particular implication for changing the distance to the last-scattering surface (Bonvin et al. 2015; Clarkson et al. 2014). None the less, this is not its only consequence. Let us assume that photons move with the effective speed of the perturbed metric but follow radial geodesics of the unperturbed FLRW geometry. A photon following perturbed geodesics has a varying effective velocity, sometimes it overtakes an idealized photon that follows a FLRW geodesic and other times it gets left behind. Consequently, they would encounter the same structure at different evolutionary stages. Since this time difference depends on the potentials the photon underwent before, it is also an integrated effect.

The growth of potentials is determined by the factor D_+/a, which we expand up to second order to quantify the temporal Born correction,

$$\left.\frac{D_+(a)}{a}\right| \approx \frac{D_+(a)}{a} + \frac{\mathrm{d}}{\mathrm{d}a}\left(\frac{D_+(a)}{a}\right)\bigg|_a \Delta a, \tag{25}$$

where $\Delta a = a^2 H(a)\Delta t$, and the time departure is given by the difference in effective light speed from the lens to the source,

$$\Delta t = \int_{\chi'}^{\chi}\frac{\mathrm{d}\chi''}{c'} - \int_{\chi'}^{\chi}\frac{\mathrm{d}\chi''}{c} \approx 2\int_{\chi'}^{\chi}\mathrm{d}\chi''\frac{\Phi(\boldsymbol{n}\chi'';\chi'')}{c^3}\,. \tag{26}$$

Finally, the temporal Born approximation adds a second-order contribution to equation (24),

$$S_{\rm ab}^{B(2)} = \frac{2}{c^2}\frac{\mathrm{d}}{\mathrm{d}\eta}\left(\frac{D_+(a)}{a}\right)_\chi \Phi_{,\rm ab}(\boldsymbol{n}\chi;0)\int_{\chi'}^{\chi}\mathrm{d}\chi''\Phi(\boldsymbol{n}\chi'';\chi''), \tag{27}$$

which is also vanishing in the matter dominated epoch of the Universe similarly to the integrated Sachs-Wolfe (iSW) effect, since both effects have a very similar origin, again due to the null property of photons.

4.4 Gravitomagnetic effect

The most general energy-momentum tensor compatible with the cosmological symmetries, is the energy-momentum tensor of a perfect fluid, for which one finds

$$T^{\alpha\beta} = (\rho c^2 + p)\upsilon^\alpha\upsilon^\beta - pg^{\alpha\beta}, \tag{28}$$

where ρ is the mass density and p the fluids pressure, both measured in a reference frame with a normalized four-velocity $\upsilon^\alpha = (\upsilon^0, \boldsymbol{\upsilon})$. Under the assumption that the gravitational lenses are slowly moving, the kinetic contribution to gravity can be ignored and the dominant component is $T^{00} = \rho c^2$. We study the validity of this assumption (Sereno 2003; Schäfer & Bartelmann 2006), considering the contribution of $T^{0i} = c\rho\upsilon^i$. It can be shown that the effective speed of light gains an additional term (Dodelson et al. 2005),

$$c' = c - \frac{2\Phi}{c} + \frac{4}{c^2}A_\parallel, \tag{29}$$

where the line-of-sight component of the vectorial mode is given by

$$A_\parallel(\boldsymbol{x},t) = -G\int\frac{\rho(\boldsymbol{x}',t)\upsilon_\parallel(\boldsymbol{x}',t)}{|\boldsymbol{x}-\boldsymbol{x}'|}\mathrm{d}\boldsymbol{x}'. \tag{30}$$

As a consequence, the second-order correction to the lensing potential is

$$S_{\rm ab}^{G(2)} = -\frac{2}{c}A_\parallel(\boldsymbol{n}\chi;\chi). \tag{31}$$

Dodelson et al. (2005) investigated this effect analytically along with Born corrections and lens–lens coupling, and it was found to be small.

5 CORRECTIONS TO WEAK-LENSING SPECTRA

We will now calculate the corrections to the weak-lensing convergence spectrum equation (15) subject to the effects described in Section 5. For this purpose, we write the lensing potential weighted by a probability distribution $p(z)$ in the ith tomographic bin as

$$\overline{\psi}_{\rm i}(\boldsymbol{n}) = \int_0^{\chi_H} {\rm d}\chi\; p_{\rm i}(z)\frac{{\rm d}z}{{\rm d}\chi}\psi(\boldsymbol{n},\chi) = \frac{2}{c^2}\int_0^{\chi_H}{\rm d}\chi\int_\chi^{\chi_H}{\rm d}\chi'\, g_{\rm i}(\chi,\chi')S_{\rm ab}((\boldsymbol{n}\chi';\chi'),(\boldsymbol{n}\chi;\chi)). \tag{32}$$

Accordingly, the averaged convergence is

$$\overline{\kappa}_{\rm i}(\boldsymbol{n}) = \frac{1}{c^2}\int_0^{\chi_H}{\rm d}\chi\int_\chi^{\chi_H}{\rm d}\chi'\, g_{\rm i}(\chi,\chi')S_{\rm aa}[(\boldsymbol{n}\chi';\chi'),(\boldsymbol{n}\chi;\chi)]. \tag{33}$$

The corresponding convergence power spectrum is

$$\begin{aligned} C_{\rm ij}(\ell) &= \int\frac{{\rm d}^2\ell'}{(2\pi)^2}\left\langle\hat{\overline{\kappa}}_{\rm i}(\boldsymbol{\ell})\hat{\overline{\kappa}}^*_{\rm j}(\boldsymbol{\ell}')\right\rangle \\ &= \frac{1}{c^4}\int\frac{{\rm d}^2\ell'}{(2\pi)^2}\int_0^{\chi_H}{\rm d}\chi_1\int_{\chi_1}^{\chi_H}{\rm d}\chi_1' g_{\rm i}(\chi_1,\chi_1')\int_0^{\chi_H}{\rm d}\chi_2\int_{\chi_2}^{\chi_H}{\rm d}\chi_2' g_{\rm j}(\chi_2,\chi_2')\left\langle\hat{S}_{\rm aa}(\boldsymbol{\ell},\chi_1,\chi_1')\hat{S}^*_{\rm aa}(\boldsymbol{\ell}',\chi_2,\chi_2')\right\rangle, \end{aligned} \tag{34}$$

where a hat denotes the 2D Fourier transform, we will not use this notation in the following if the argument to the Fourier variable is given and no confusion arises. In the computation of the convergence power spectra, two approximations have been made: the first corresponds to the flat sky approximation, valid for small angles, where we expect a stronger correlation between distorted images. The second one is the Limber approximation, in which we ignore any correlation along the line of sight, implying that the power spectrum of density fluctuations $P_\delta(k)$ can be evaluated at $k=\ell/\chi$. For more information on common approximations made in cosmic shear, we refer to Kitching et al. (2017).

Furthermore, we note that second-order corrections involve products of two statistical fields in position space, which will give rise to convolutions in Fourier space. In the following, we present the obtained autocorrelation power spectra for the different effects, and refer the reader to the appendix for the cross-correlations for sake of readability.

5.1 Sachs–Wolfe effect

The 2D power spectrum of the averaged convergence for the Sachs–Wolfe correction is, using equation (20),

$$C^{\rm S}_{\rm ii}(\ell) = \frac{1}{c^6}\int_0^{\chi_H}\frac{{\rm d}\chi}{\chi^2}\int\frac{{\rm d}^2\ell'}{(2\pi)^2}(\ell')^4 M_{\rm ij}(\ell',|\boldsymbol{\ell}-\boldsymbol{\ell}'|;\chi), \tag{35}$$

where we abbreviated the mode coupling integral:

$$M^{\rm S}_{\rm ij}(\ell,\ell';\chi) = \int_\chi^{\chi_H}\frac{{\rm d}\chi'}{(\chi')^2}d_{\rm i}(\chi')d_j(\chi')P_\Phi\left(\frac{\ell}{\chi};\chi\right)P_\Phi\left(\frac{\ell'}{\chi'};\chi'\right). \tag{36}$$

with $d_{\rm i}(\chi') = \frac{p_i(\chi')}{H(a(\chi'))}\frac{1}{\chi'^2}$. Clearly, we couple the potential power spectrum and two different scales and two different times. Due to the comoving distances in the denominator, this effect will be important only on large scales.

5.2 Peculiar velocities

In case of peculiar motions only, the projection of the velocity along the line of sight introduces a correction. In this case, the Limber approximation cannot be applied directly, since it assumes that there is no correlation between parallel modes. The final result is,

$$C^{\rm V}_{\rm ij}(\ell) = \frac{1}{c^4}\int_0^{\chi_H}\frac{{\rm d}\chi}{\chi^2}\int\frac{{\rm d}k'}{2\pi^2}M_{\rm ij}(k',\ell;\chi). \tag{37}$$

with mode coupling integral,

$$M^{\rm V}_{\rm ij}(k',\ell;\chi) = \chi^2\int_\chi^{\chi_H}{\rm d}\chi'\frac{{\rm d}D_+(a)}{{\rm d}\eta}d_{\rm i}(\chi')\int_\chi^{\chi_H}{\rm d}\chi''\frac{{\rm d}D_+(a)}{{\rm d}\eta}d_{\rm j}(\chi'')P_\delta\left(k';\chi\right)P_\delta\left(\frac{\sqrt{\ell^2+(k'\chi')^2)}}{\chi};0\right)j_0''(k'|\chi'-\chi''|). \tag{38}$$

Comparing this correction to the one produced by the Sachs–Wolfe effect (35), we find two structural differences even though both effects are local. First, the convolution is restricted to modes perpendicular to $\boldsymbol{\ell}$. Secondly, there is no delta function between the primed comoving distances, instead we find a Bessel function which is a broader kernel, since velocities are originated by gradients of potentials and therefore their correlation length is larger.

5.3 Integrated Sachs–Wolfe effect

For the integrated Sachs–Wolfe, we obtain two different terms,

$$C^{\rm I}_{\rm ij}(\ell) = \frac{4}{c^8}\int_0^{\chi_H}\frac{{\rm d}\chi}{\chi^2}\int\frac{{\rm d}^2\ell'}{(2\pi)^2}\left((\ell')^4 M_{1,\,\rm ij}(\ell',|\boldsymbol{\ell}-\boldsymbol{\ell}'|;\chi)+(\ell')^2|\boldsymbol{\ell}-\boldsymbol{\ell}'|^2 M_{2,\,\rm ij}(\ell',|\boldsymbol{\ell}-\boldsymbol{\ell}'|;\chi)\right). \tag{39}$$

with two mode coupling integrals

$$M^{\mathrm{I}}_{1,\,\mathrm{ij}}(\ell,\ell';\chi)=\int_{\chi}^{\chi_H}\mathrm{d}\chi_1' d_{\mathrm{i}}(\chi_1')\int_{\chi}^{\chi_H}\mathrm{d}\chi_2' d_j(\chi_2')\int_{\chi}^{\min(\chi_1',\chi_2')}\frac{\mathrm{d}\chi''}{(\chi'')^2}\left(\frac{\mathrm{d}}{\mathrm{d}\eta}\left(\frac{D_+(a)}{a}\right)\right)^2_{\chi''}P_\Phi\left(\frac{\ell}{\chi};\chi\right)P_\Phi\left(\frac{\ell'}{\chi''};0\right) \tag{40}$$

and

$$\begin{aligned}M^{\mathrm{I}}_{2,\,ij}(\ell,\ell';\chi)=&\left(\frac{D_+(a)}{a}\right)_{\chi}\frac{\mathrm{d}}{\mathrm{d}\eta}\left(\frac{D_+(a)}{a}\right)_{\chi}\int_{\chi}^{\chi_H}\mathrm{d}\chi_1' d_{\mathrm{i}}(\chi_1')\int_{\chi}^{\chi_H}\mathrm{d}\chi_2' d_j(\chi_2')\\&\times\int_{\chi}^{\min(\chi_1',\chi_2')}\frac{\mathrm{d}\chi''}{(\chi'')^2}\left(\frac{D_+(a)}{a}\right)_{\chi''}\frac{\mathrm{d}}{\mathrm{d}\eta}\left(\frac{D_+(a)}{a}\right)_{\chi''}P_\Phi\left(\frac{\ell}{\chi};0\right)P_\Phi\left(\frac{\ell'}{\chi''};0\right).\end{aligned} \tag{41}$$

Both integrals depend on the change of the growth factor and thus are sensitive to the time evolution of the potentials opposed to equation (35), due to the integration of the effect along the line of sight. However, the scaling compared to equation (35) is similar so that we expect the effect to be highest on very large scales.

5.4 Second-order corrections to light propagation

Since the second-order correction to the light propagation only involves additional autocorrelations of the potential, i.e. correlations at the same positions or comoving distance, the Limber approximation can be applied directly after applying Wicks theorem to compute the correlation in the limit of Gaussian fields. Therefore, we get:

$$C^{\mathrm{P}}_{\mathrm{ij}}(\ell)=\frac{2\ell^4}{c^8}\int_0^{\chi_H}\frac{\mathrm{d}\chi}{\chi^2}\left(\int\frac{\mathrm{d}^3k'}{(2\pi)^3}M_{\mathrm{ij}}(k',|\boldsymbol{k}-\boldsymbol{k}'|;\chi)\right)_{k=\frac{\ell}{\chi}}, \tag{42}$$

with mode coupling integral,

$$M^{\mathrm{P}}_{\mathrm{ij}}(k,k';\chi)=\int_{\chi}^{\chi_H}\mathrm{d}\chi' g_{\mathrm{i}}(\chi,\chi')\int_{\chi}^{\chi_H}\mathrm{d}\chi'' g_{\mathrm{j}}(\chi,\chi'')P_\Phi(k;\chi)\,P_\Phi\left(k';\chi\right). \tag{43}$$

It should be noted that the mode coupling integral depends on the wave vector directly and that $k=\ell/\chi$ is only inserted afterwards as opposed to the other corrections. The reason for this is exactly that we only apply the Limber projection in the very last step, as for normal cosmic shear power spectra.

5.5 Temporal Born approximation

The temporal Born corrections works very similar to the iSW corrections. We find:

$$C^{\mathrm{B}}_{\mathrm{ij}}(\ell)=\frac{4}{c^{10}}\int_0^{\chi_H}\frac{\mathrm{d}\chi}{\chi^2}\left(\frac{\mathrm{d}}{\mathrm{d}\eta}\left(\frac{D_+(a)}{a}\right)\right)^2_{\chi}\int\frac{\mathrm{d}^2\ell'}{(2\pi)^2}(\ell')^4 M_{\mathrm{ij}}(\ell',|\boldsymbol{\ell}-\boldsymbol{\ell}'|;\chi), \tag{44}$$

with mode coupling integral,

$$M^{\mathrm{B}}_{\mathrm{ij}}(\ell,\ell';\chi)=\int_{\chi}^{\chi_H}\mathrm{d}\chi_1' g_{\mathrm{i}}(\chi,\chi_1')\int_{\chi}^{\chi_H}\mathrm{d}\chi_2' g_{\mathrm{j}}(\chi,\chi_2')\int_{\chi}^{\min(\chi_1',\chi_2')}\frac{\mathrm{d}\chi''}{(\chi'')^2}P_\Phi\left(\frac{\ell}{\chi};0\right)P_\Phi\left(\frac{\ell'}{\chi''};\chi''\right). \tag{45}$$

Compared to the other effects, we already see that it will be weaker due to the pre-factor of c^{-10} and it will be highest on large scales as well like the SW and iSW contributions.

5.6 Gravitomagnetic corrections

Finally, we investigate the effect of moving lenses and thus the autocorrelation of the gravitomagnetic correction:

$$C^{\mathrm{G}}_{\mathrm{ij}}(\ell)=\frac{4}{c^6}\int_0^{\chi_H}\mathrm{d}\chi\left(\chi\frac{\mathrm{d}D_+(a)}{\mathrm{d}\eta}\right)^2\left[\int\frac{\mathrm{d}k'}{(2\pi)^2}|\boldsymbol{k}-\boldsymbol{k}'|^4 M_{\mathrm{ij}}(k',|\boldsymbol{k}-\boldsymbol{k}'|;\chi)\right]_{k=l/\chi}, \tag{46}$$

where the mode coupling integral is given by

$$M^{\mathrm{G}}_{\mathrm{ij}}(k',|\boldsymbol{k}-\boldsymbol{k}'|;\chi)=\int_{\chi}^{\chi_H}\mathrm{d}\chi' g_{\mathrm{i}}(\chi,\chi')\int_{\chi}^{\chi_H}\mathrm{d}\chi'' g_{\mathrm{j}}(\chi,\chi'')P_\delta(k;0)\int_{-1}^{1}\mathrm{d}\mu\left(\mu^2+\frac{k'\mu(k-k'\mu)}{|\boldsymbol{k}-\boldsymbol{k}'|^2}\right)P_\Phi\left(|\boldsymbol{k}-\boldsymbol{k}'|;\chi\right). \tag{47}$$

Which will have the largest impact of the computed effects, which can be again seen by considering the pre-factor, which is only c^{-6} here. Furthermore, it should be noted that the integrand of the mode coupling function depends of the orientation of the different wave vectors for which the correlation is formed, which is then averaged over.

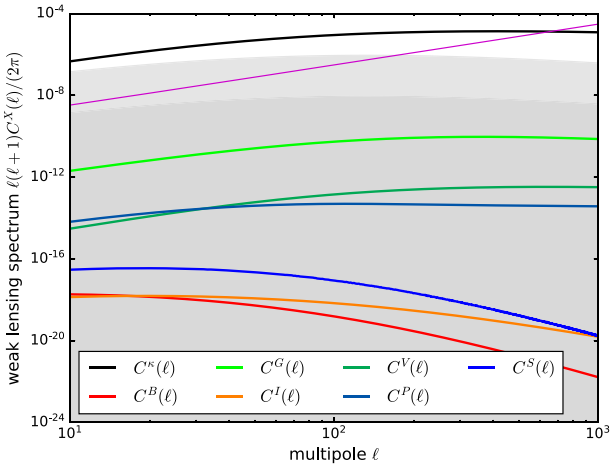

Figure 1. Angular autospectra $C^X(\ell)$ for 2D weak lensing: temporal Born effect (red) and the integrated Sachs–Wolfe effect (orange), and the result for linear weak lensing (black) in comparison, *Euclid*'s shape noise (solid line for the actual value $\sigma_\epsilon^2/\bar{n}$, dashed line for $10^{-2}\sigma_\epsilon^2/\bar{n}$, magenta), and the cosmic variance limit $\Delta C^\kappa(\ell) = \sqrt{2/(2\ell+1)}C^\kappa(\ell)$ (grey bands for the actual cosmic variance and 10^{-2}) of that value). In addition, the corrections due to gravitomagnetic effects ($C^G(\ell)$ in green), peculiar velocities ($C^V(\ell)$, dark green), higher order corrections to the speed of propagation ($C^S(\ell)$, blue) are plotted.

5.7 Results

In Fig. 1, the autocorrelations calculated in the last section are shown. The black line shows the linear angular power spectrum, while the magenta line represents the shape-noise contribution, and the grey band represents cosmic variance. Clearly the corrections lie well below the shape noise and within the effect of cosmic variance. The largest effect stamps from gravitomagnetic effects. Figs 2 and 3 show the cross-correlations (see Appendix) between the different effects again shown together with the lensing spectrum, cosmic variance, and shape noise.

We calculate the Fisher matrix

$$F_{\mu\nu} = f_{\rm sky}\sum_\ell \frac{2\ell+1}{2}\,{\rm tr}\left(\boldsymbol{C}^{-1}(\ell)\partial_\mu \boldsymbol{C}(\ell)\,\boldsymbol{C}^{-1}(\ell)\partial_\nu \boldsymbol{C}(\ell)\right), \tag{48}$$

where $\boldsymbol{C}$ is the tomographic covariance matrix consisting of the sum lensing power spectrum, the shape noise, and all corrections terms. The sky coverage for *Euclid* is roughly 15000 deg^2. Next, we are trying to fit a true model, $\boldsymbol{C}$, with a wrong model $\boldsymbol{C}_{\rm f}$, not including the corrections. The bias δ_μ is given by (Taburet et al. 2009)

$$\delta_\mu = (\boldsymbol{G}^{-1})_{\mu\nu}a^\nu, \tag{49}$$

where

$$a^\nu = \left\langle \frac{\partial L_{\rm f}}{\partial\theta_\nu}\right\rangle, \quad G_{\mu\nu} = -\left\langle \frac{\partial^2 L_{\rm f}}{\partial\theta^\mu\partial\theta^\nu}\right\rangle, \tag{50}$$

to be evaluated at the true model. $L_{\rm f}$ refers to the log-likelihood of the false model. The parameter estimation process for a wCDM model from a tomographic survey with five bins and the anticipated redshift distribution of *Euclid*'s weak-lensing data, we arrive at typical systematic errors of $\simeq 10^{-5}$ for $\Omega_{\rm m}$, σ_8, h, and w, and of the order $\simeq 10^{-6}$ for $n_{\rm s}$, which is certainly well below the statistical error, consistent with the absolute values found for the correction.

6 SUMMARY

The subject of our investigation were gravitational secondary contributions to the weak-lensing signal. These include as local effects (i) the Sachs–Wolfe effect due to the non-zero gravitational potential where the lensed galaxy is situated, (ii) contributions to the total redshift if the lensed galaxy has a non-zero peculiar velocity relative to the Hubble flow, corrections due to general relativity in the weak field limit because of (iii) quadratic corrections to the effective speed of propagation, and (iv) gravitomagnetic terms due to the contributions of the momentum density to the gravitational field. As integrated effects, we considered (v) the integrated Sachs–Wolfe effect affecting the redshift of the lensed galaxy and, in addition, we evaluate the effect of the non-uniform effective speed of light in gravitational potentials that gives rise to an equivalent correction corresponding to Born corrections. As photons are travelling along null geodesics from a source galaxy to the observer, their effective speed of propagation is modulated by the depth of the gravitational potentials that they need to traverse. Consequently, they encounter deflecting structures at a different time and therefore at a different stage of structure formation in comparison to idealized photons which follow null geodesics of an FLRW space–time.

These corrections are computed for an FLRW cosmology with weak perturbations which source gravitational potentials that are effectively Newtonian. Structure formation was treated in the linear limit, which enforces near-Gaussian statistics of the gravitational

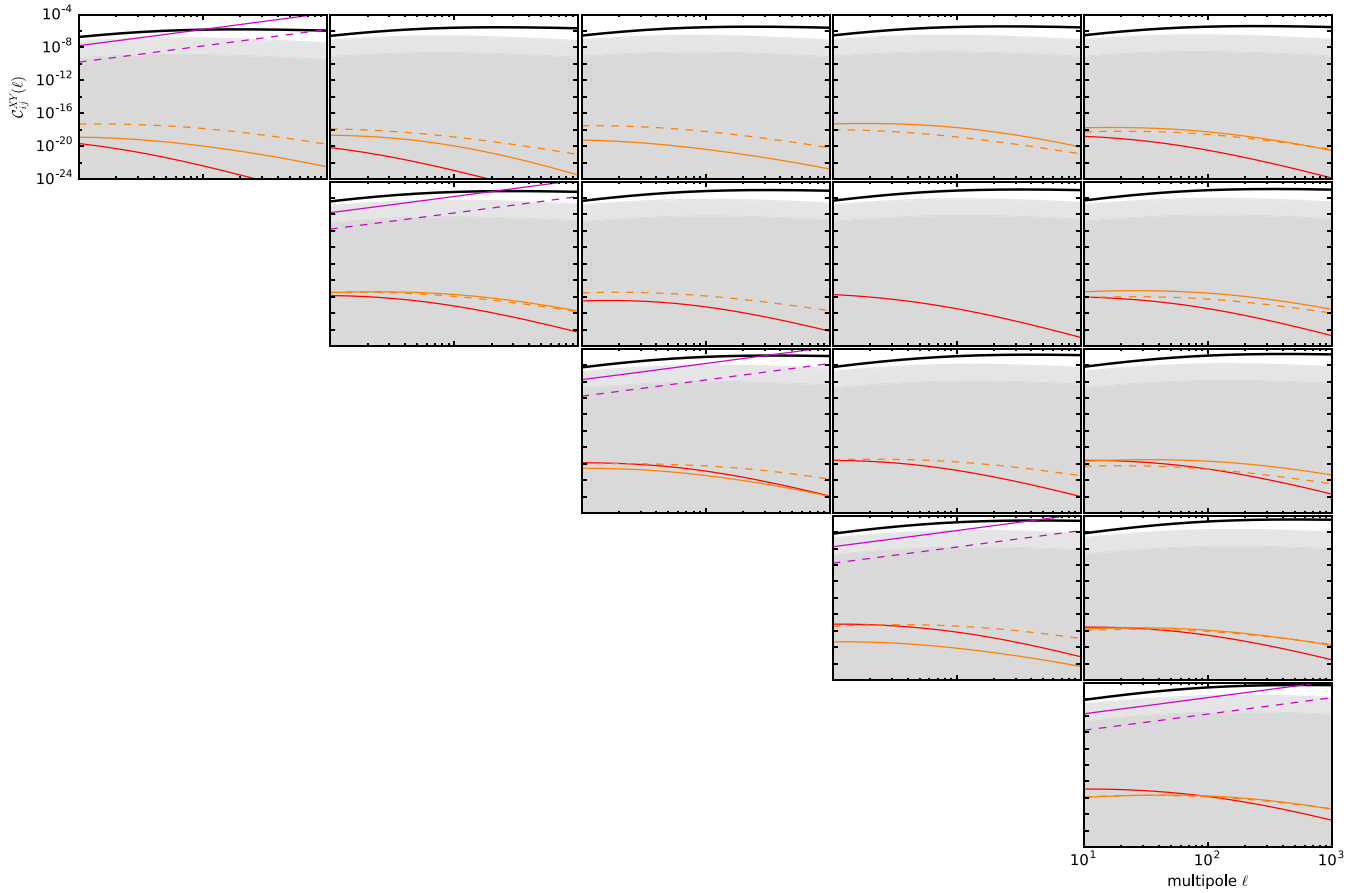

Figure 2. Angular spectra $C_{\rm ij}^{XY}(\ell)$ for five-bin tomography in the representation $\mathcal{C}_{\rm ij}^{XY}(\ell) = \ell(\ell+1)C_{\rm ij}^{XY}(\ell)/(2\pi)$: temporal Born effect (solid line, red) and the integrated Sachs–Wolfe effect (dashed line, orange), and the cross-correlation between the two effects. For comparison, we show the result for linear weak lensing (solid line, black), *Euclid*'s shape noise (solid line for the actual value $\sigma_\epsilon^2 n_{\rm bin}/\bar{n}$, dashed line for $10^{-2}\sigma_\epsilon^2 n_{\rm bin}/\bar{n}$, magenta) and the cosmic variance limit $\Delta C_{\rm ij}^{\kappa}(\ell) = \sqrt{2/(2\ell+1)}C_{\rm ij}^{\kappa}(\ell)$ (grey bands for the actual cosmic variance and 10^{-2} of that value).

potential fluctuations. From this model of linear and Gaussian perturbations, we derive angular spectra of all correction terms and their cross-correlations in perturbation theory, where the non-linear dependencies of all effects on the fundamental fields would cause non-Gaussian statistical properties. We carry out our computation for the characteristics of the *Euclid* survey, but a similar strength of the correction terms for the weak-lensing signal should be applicable for any reasonably deep weak-lensing survey.

There is the general tendency that effects related to peculiar velocities, either of the source galaxies leading to a change in redshift relative to the cosmological one or of the lensing structure giving rise to gravitomagnetic effects, provide the largest corrections, followed by effects involving the gravitational potential at the lens, i.e. higher order corrections to the light propagation, or due to the LSS into which the source galaxy is embedded, causing a gravitational redshift. The smallest effects are integrated effects depending on the evolution of the gravitational potentials, which are interpreted as an integrated Sachs–Wolfe effect or the temporal Born correction. The latter two effects show the same phenomenology in terms of cosmological parameters and would be absent in a flat, matter-dominated cosmology with $\Omega_{\rm m} = 1$. There, the growth function $D_+(a)$ is equal to the scale factor a and consequently, fluctuations in the gravitational potential are constant and do not give rise to integrated effects. We find the conceptual difference between these two effects striking, in particular because they give at the same time rise to very similar expressions and show identical dependencies on cosmological parameters.

The computation was done for a wCDM cosmology and the magnitude of the correction terms in comparison to the linear weak lensing is $10^{-5\ldots-6}$ at most, indicating that the most important secondary effects in weak lensing are in fact reduced shear and magnification corrections (Krause & Hirata 2010), intrinsic alignments (Blazek et al. 2015; Joachimi et al. 2015; Kiessling et al. 2015; Kirk et al. 2015; Troxel & Ishak 2015; Schaefer & Merkel 2017), and uncertainties in the redshift distribution (e.g. Abrahamse et al. 2011). We would argue that the magnitude of the effects does not strongly depend on the particular dark energy model and should be valid for a ΛCDM cosmology as well. Due to the smallness of the individual effects in comparison to the linear weak-lensing signal and the shape noise implies that there should be a negligible effect on the estimation of cosmological parameters. We compute the resulting systematic errors and found them to be very small.

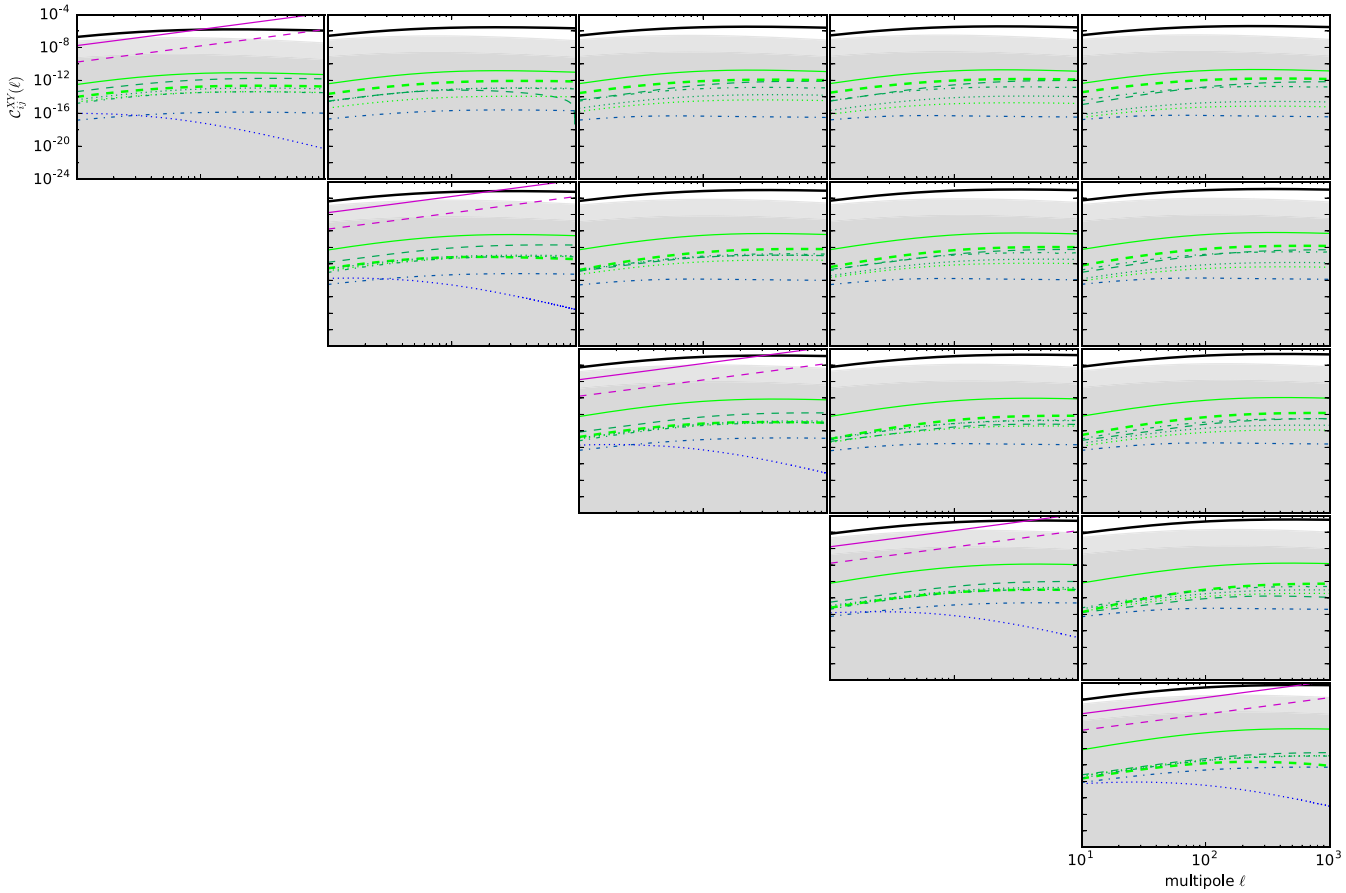

Figure 3. Angular spectra $C_{\rm ij}^{XY}(\ell)$ for five-bin tomography in the representation $\mathcal{C}_{\rm ij}^{XY}(\ell) = \ell(\ell+1)C_{\rm ij}^{XY}(\ell)/(2\pi)$: gravitomagnetic corrections (solid line, green) and peculiar velocity corrections (dashed line, light green), corrections due to post-Newtonian potentials (dash-dotted line, light blue), Sachs–Wolfe effect (dotted line, blue), and all cross-correlations. For comparison, we show the result for linear weak lensing (solid line, black), *Euclid*'s shape noise (solid line for the actual value $\sigma_\epsilon^2 n_{\rm bin}/\bar{n}$, dashed line for $10^{-2}\sigma_\epsilon^2 n_{\rm bin}/\bar{n}$, magenta), and the cosmic variance limit $\Delta C_{\rm ij}^{\kappa}(\ell) = \sqrt{2/(2\ell+1)}C_{\rm ij}^{\kappa}(\ell)$ (grey bands for the actual cosmic variance and 10^{-2} of that value).

ACKNOWLEDGEMENTS

We would like to thank P. Norberg for giving us the opportunity to write up this project. RR acknowledges funding by the graduate college Astrophysics of cosmological probes of gravity by Landesgraduiertenakademie Baden-Württemberg. We thank the anonymous referee for requesting clarifications on some points, which made our paper more accessible.

REFERENCES

Abrahamse A., Knox L., Schmidt S., Thorman P., Tyson J. A., Zhan H., 2011, ApJ, 734, 36
Amara A., Réfrégier A., 2007, MNRAS, 381, 1018
Amara A., Réfrégier A., 2008, MNRAS, 391, 228
Bacon D. J., Refregier A. R., Ellis R. S., 2000, MNRAS, 318, 625
Bartelmann M., 2010, Class. Quantum Gravity, 27, 233001
Bartelmann M., Schneider P., 2001, Phys. Rep., 340, 291
Bender R. et al., 2000, Deep Fields. Springer-Verlag, Berlin, p. 96
Bernardeau F., Bonvin C., Vernizzi F., 2010, Phys. Rev. D, 81, 083002
Blazek J., Vlah Z., Seljak U., 2015, J. Cosmol. Astropart. Phys., 08, 15
Bolzonella M., Miralles J.-M., Pelló R., 2000, A&A, 363, 476
Bonvin C., 2008, Phys. Rev. D, 78, 123530
Bonvin C., Clarkson C., Durrer R., Maartens R., Umeh O., 2015, J. Cosmol. Astropart. Phys., 2015, 050
Bridle S., 2010, MNRAS, 405, 2044
Calabrese M., Carbone C., Fabbian G., Baldi M., Baccigalupi C., 2015, J. Cosmol. Astropart. Phys., 2015, 049
Carbone C., Baccigalupi C., Bartelmann M., Matarrese S., Springel V., 2009, MNRAS, 396, 668
Castro P. G., Heavens A. F., Kitching T. D., 2005, Phys. Rev. D, 72, 023516
Clarkson C., Umeh O., Maartens R., Durrer R., 2014, J. Cosmol. Astropart. Phys., 2014, 036
Cooray A., Hu W., 2002, ApJ, 574, 19

Croft R. A., Metzler C. A., 2000, ApJ, 545, 561
Croft R. A. C., Freeman P. E., Schuster T. S., Schafer C. M., 2017, MNRAS, 469, 4422
Cunha C. E., Huterer D., Lin H., Busha M. T., Wechsler R. H., 2014, MNRAS, 444, 129
Dodelson S., Kolb E. W., Matarrese S., Riotto A., Zhang P., 2005, Phys. Rev. D, 72, 103004
Eisenstein D. J., Hu W., 1998, ApJ, 496, 605
Eisenstein D. J., Hu W., 1999, ApJ, 511, 5
Gaztañaga E., Eriksen M., Crocce M., Castander F. J., Fosalba P., Marti P., Miquel R., Cabré A., 2012, MNRAS, 422, 2904
Giblin J. T. Jr, Mertens J. B., Starkman G. D., Zentner A. R., 2017, Phys. Rev. D, 96, 103530
Hagstotz S., Schaefer B. M., Merkel P. M., 2015, MNRAS, 454, 831
Hamilton A. J. S., 1998, Astrophysics and Space Science Library, Vol. 231, The Evolving Universe. Selected Topics on Large-Scale Structure and on the Properties of Galaxies. Kluwer Academic Publishers, Dordrecht, p. 185
Heavens A., 2003, MNRAS, 343, 1327
Hilbert S., Hartlap J., White S. D. M., Schneider P., 2009, A&A, 499, 31
Hoekstra H., Jain B., 2008, Annu. Rec. Nucl. Part. Sci., 58, 99
Hoekstra H., Viola M., Herbonnet R., 2017, MNRAS, 468, 3295
Hu W., 1999, ApJ, 522, L21
Huterer D., 2010, Gen. Relat. Grav., 42, 2177
Jain B., Seljak U., White S., 2000, ApJ, 530, 547
Joachimi B. et al., 2015, Space Sci. Rev., 193, 1
Kaiser N., 1987, MNRAS, 227, 1
Kaiser N., Wilson G., Luppino G. A., 2001, ApJ, 556, L2
Kayo I., Takada M., Jain B., 2013, MNRAS, 429, 344
Kiessling A. et al., 2015, Space Sci. Rev., 193, 67
Kilbinger M., 2015, Rep. Prog. Phys., 78, 086901
Kilbinger M. et al., 2009, A & A, 497, 677
Kirk D. et al., 2015, Space Sci. Rev., 193, 139
Kitching T. D. et al., 2014, MNRAS, 442, 1326
Kitching T. D., Alsing J., Heavens A. F., Jimenez R., McEwen J. D., Verde L., 2017, MNRAS, 469, 2737
Krause E., Hirata C. M., 2010, A&A, 523, A28
Laureijs R. et al., 2011, preprint (arXiv:1110.3193)
Lee J., 2011, ApJ, 732, 99
Lee M. H., Paczynski B., 1990, ApJ, 357, 32
Limber D. N., 1954, ApJ, 119, 655
Linder E. V., Jenkins A., 2003, MNRAS, 346, 573
LSST Science Collaboration et al., 2009, preprint (arXiv:0912.0201)
Marozzi G., Fanizza G., Di Dio E., Durrer R., 2016, J. Cosmol. Astropart. Phys., 9, 028
Miller L. et al., 2013, MNRAS, 429, 2858
Percival W. J., Samushia L., Ross A. J., Shapiro C., Raccanelli A., 2011, Phil. Trans. R. Soc. A: Math. Phys. Eng. Sci., 369, 5058
Petri A., Haiman Z., May M., 2017, Phys. Rev. D, 95, 123503
Pratten G., Lewis A., 2016, J. Cosmol. Astropart. Phys., 2016, 047
Sachs R. K., Wolfe A. M., 1967, ApJ, 147, 73
Schaefer B. M., Merkel P. M., 2017, MNRAS, 3, 3453
Schäfer B. M., Bartelmann M., 2006, MNRAS, 369, 425
Schäfer B. M., Heisenberg L., 2012, MNRAS, 423, 3445
Schäfer B. M., Heisenberg L., Kalovidouris A. F., Bacon D. J., 2012, MNRAS, 420, 455
Schneider P., Weiss A., 1988, ApJ, 330, 1
Seitz S., Schneider P., 1994, A&A, 287, 349
Sereno M., 2003, Phys. Rev. D, 67, 064007
Shapiro C., Cooray A., 2006, J. Cosmol. Astropart. Phys., 0603, 007
Taburet N., Aghanim N., Douspis M., Langer M., 2009, MNRAS, 392, 1153
Takada M., White M., 2004, ApJ, 601, L1
Tansella V., Bonvin C., Durrer R., Ghosh B., Sellentin E., 2017, J. Cosmol. Astropart. Phys., 3, 019
Troxel M. A., Ishak M., 2015, Phys. Rep., 558, 1
Van Waerbeke L. et al., 2000, A&A, 358, 30
Wang L., Steinhardt P. J., 1998, ApJ, 508, 483

APPENDIX: CROSS-CORRELATIONS

We summarize the cross-correlations for all effects considered in Section 5, which are expected to be non-zero due to the fact that all originate from the same random field and are thus jointly described by the power spectrum of potential fluctuations. We will use the following abbreviations: Sachs–Wolfe effect (S), integrated Sachs–Wolfe effect (I), temporal Born corrections (T), peculiar velocity corrections (V), gravitomagnetic corrections (G), and second-order light propagation (P). All spectra are given in the tomographic bins i and j.

A1 Redshift space distortions cross-correlations

Note that we are considering redshift space distortions on the source galaxy redshift. Hence, they correct the gravitational potential in the same way (equation 18). Furthermore, they all depend on the gravitational field or its parallel derivative, and thus we expect a non-zero cross-correlation between them.

The cross-correlation between the Sachs–Wolfe effect and the integrated Sachs–Wolfe effect gives

$$C_{\rm ij}^{\rm SI}(\ell) = \frac{2}{c^7}\int_0^{\chi_H}\frac{{\rm d}\chi}{\chi^2}\int\frac{{\rm d}^2\ell'}{(2\pi)^2}\left((\ell')^4 M_{1,\,\rm ij}^{\rm SI}(\ell', |\boldsymbol{\ell}-\boldsymbol{\ell}'|;\chi) + (\ell')^2|\boldsymbol{\ell}-\boldsymbol{\ell}'|^2 M_{2,\,\rm ij}^{\rm SI}(\ell', |\boldsymbol{\ell}-\boldsymbol{\ell}'|;\chi)\right), \tag{A1}$$

where

$$M_{1,\,\rm ij}^{\rm SI}(\ell,\ell';\chi) = \int_\chi^{\chi_H}{\rm d}\chi' d_{\rm i}(\chi')\int_\chi^{\chi'}\frac{{\rm d}\chi''}{(\chi'')^2}\left(\frac{D_+(a)}{a}\right)_{\chi''}\frac{\rm d}{{\rm d}\eta}\left(\frac{D_+(a)}{a}\right)_{\chi''} d_{\rm j}(\chi'')P_\Phi\left(\frac{\ell}{\chi};\chi\right)P_\Phi\left(\frac{\ell'}{\chi''};0\right), \tag{A2}$$

$$M_{2,\,\rm ij}^{\rm SI}(\ell,\ell';\chi) = \int_\chi^{\chi_H}{\rm d}\chi_1' d_{\rm j}(\chi')\int_0^{\chi}\frac{{\rm d}\chi''}{(\chi'')^2}\left(\frac{D_+(a)}{a}\right)_{\chi''}\frac{\rm d}{{\rm d}\eta}\left(\frac{D_+(a)}{a}\right)_{\chi''} P_\Phi\left(\frac{\ell}{\chi};\chi\right)P_\Phi\left(\frac{\ell'}{\chi''};0\right). \tag{A3}$$

On the other hand, the cross-correlation between the Sachs–Wolfe effect and the peculiar velocities effect is

$$C_{\rm ij}^{\rm SP}(\ell) = -\frac{1}{c^5}\int_0^{\chi_H}\frac{{\rm d}\chi}{\chi^2}\int\frac{{\rm d}k'}{2\pi^2}M_{\rm ij}^{\rm SP}(k',\ell;\chi), \tag{A4}$$

with

$$M_{\rm ij}^{\rm SP}(k',\ell;\chi) = \int_\chi^{\chi_H}{\rm d}\chi' d_{\rm i}(\chi')\left(\frac{{\rm d}D_+(a)}{{\rm d}\eta}\right)_{\chi'}\int_\chi^{\chi_H}{\rm d}\chi''\left(\frac{D_+(a)}{a}\right)_{\chi''} d_{\rm j}(\chi'')k'(\ell^2+(k'\chi')^2)^2$$
$$\times P_{\Phi\delta}\left(k';0\right)P_\Phi\left(\frac{\sqrt{\ell^2+(k'\chi')^2}}{\chi};\chi\right)j_0'(k'|\chi'-\chi''|). \tag{A5}$$

Finally, the cross-correlation between the integrated Sachs–Wolfe effect and the peculiar velocities effect is

$$C_{\rm ij}^{\rm IV}(\ell) = -\frac{2}{c^6}\int_0^{\chi_H}\frac{{\rm d}\chi}{\chi^2}\int\frac{{\rm d}k'}{2\pi^2}M_{\rm ij}^{\rm IV}(k',\ell;\chi), \tag{A6}$$

with

$$M_{\rm ij}^{\rm IV}(k',\ell;\chi) = \int_\chi^{\chi_H}{\rm d}\chi_1' d_{\rm i}(\chi_1')\frac{\rm d}{{\rm d}\eta}\left(\frac{D_+(a)}{a}\right)_{\chi_1'}\int_\chi^{\chi_H}{\rm d}\chi_2' d_{\rm j}(\chi_2')\int_0^{\chi_1'}{\rm d}\chi''\left(\frac{D_+(a)}{a}\right)_{\chi''}k'(\ell^2+(k'\chi_1')^2)^2$$
$$\times P_{\Phi\delta}\left(k';0\right)P_\Phi\left(\frac{\sqrt{\ell^2+(k'\chi_1')^2}}{\chi};\chi\right)j_0'(k'|\chi_1'-\chi''|). \tag{A7}$$

A2 Redshift space distortions cross-correlations with temporal Born effect

The temporal Born-effect correction is very similar to the integrated Sachs–Wolf effect one, since they both depend on the time derivative of the gravitational potential and share a similar structure. Hence, we expect that the temporal Born correction is correlated with the redshift space distortions ones.

The cross-correlation between the integrated Sachs–Wolfe effect and the temporal Born effect is

$$C_{\rm ij}^{\rm IB}(\ell) = -\frac{4}{c^9}\int_0^{\chi_H}\frac{{\rm d}\chi}{\chi^2}\int\frac{{\rm d}^2\ell'}{(2\pi)^2}\left((\ell')^4 M_{1,\,\rm ij}^{\rm IB}(\ell', |\boldsymbol{\ell}-\boldsymbol{\ell}'|;\chi) + (\ell')^2|\boldsymbol{\ell}-\boldsymbol{\ell}'|^2 M_{2,\,\rm ij}^{\rm IB}(\ell', |\boldsymbol{\ell}-\boldsymbol{\ell}'|;\chi)\right), \tag{A8}$$

with

$$M_{1,\,\rm ij}^{\rm IB}(\ell,\ell';\chi) = \frac{\rm d}{{\rm d}\eta}\left(\frac{D_+(a)}{a}\right)_\chi\left(\frac{D_+(a)}{a}\right)_\chi\int_\chi^{\chi_H}{\rm d}\chi_1' d_{\rm i}(\chi_1')$$
$$\times\int_\chi^{\chi_1'}\frac{{\rm d}\chi''}{(\chi'')^2}\frac{\rm d}{{\rm d}\eta}\left(\frac{D_+(a)}{a}\right)_{\chi''}\left(\frac{D_+(a)}{a}\right)_{\chi''}\Phi(\chi'')\int_{\chi''}^{\chi_H}{\rm d}\chi_2' g_j(\chi,\chi_2')P_\Phi\left(\frac{\ell}{\chi};0\right)P_\Phi\left(\frac{\ell'}{\chi''};0\right), \tag{A9}$$

and

$$M_{2,\,\rm ij}^{\rm IB}(\ell,\ell';\chi) = \int_\chi^{\chi_H}{\rm d}\chi_1' d_{\rm i}(\chi_1')\int_0^{\chi}\frac{{\rm d}\chi''}{(\chi'')^2}\left(\frac{\rm d}{{\rm d}\eta}\left(\frac{D_+(a)}{a}\right)_{\chi''}\right)^2\int_\chi^{\chi_H}{\rm d}\chi_2' g_{\rm j}(\chi,\chi_2')P_\Phi\left(\frac{\ell}{\chi};\chi\right)P_\Phi\left(\frac{\ell'}{\chi''};0\right). \tag{A10}$$

The Sachs–Wolfe effect and temporal Born-effect cross-correlation is

$$C_{\rm ij}^{\rm SB}(\ell) = -\frac{2}{c^8}\int_0^{\chi_H}\frac{{\rm d}\chi}{\chi^2}\int\frac{{\rm d}^2\ell'}{(2\pi)^2}(\ell')^4 M_{\rm ij}^{\rm SB}(\ell', |\boldsymbol{\ell}-\boldsymbol{\ell}'|;\chi), \tag{A11}$$

with

$$M_{\rm ij}^{\rm SB}(\ell,\ell';\chi)=\left(\frac{D_+(a)}{a}\right)_\chi\frac{\rm d}{{\rm d}\eta}\left(\frac{D_+(a)}{a}\right)_\chi\int_\chi^{\chi_H}{\rm d}\chi'\frac{d_{\rm i}(\chi')}{\chi'^2}\int_{\chi'}^{\chi_H}{\rm d}\chi''g_{\rm j}(\chi,\chi'')P_\Phi\left(\frac{\ell}{\chi};0\right)P_\Phi\left(\frac{\ell'}{\chi'};\chi'\right). \tag{A12}$$

Finally, the cross-correlation between the peculiar motions and the temporal Born effect is

$$C_{\rm ij}^{\rm BV}(\ell)=\frac{2}{c^7}\int_0^{\chi_H}\frac{{\rm d}\chi}{\chi^2}\int\frac{{\rm d}k'}{2\pi^2}k'M_{\rm ij}^{\rm BV}(k',\ell;\chi), \tag{A13}$$

with

$$\begin{aligned}M_{\rm ij}^{\rm BV}(k',\ell;\chi)=&\frac{\rm d}{{\rm d}\eta}\left(\frac{D_+(a)}{a}\right)_\chi\left(\frac{D_+(a)}{a}\right)_\chi\int_\chi^{\chi_H}{\rm d}\chi_1'g_{\rm i}(\chi,\chi_1')\int_\chi^{\chi_1'}{\rm d}\chi''\left(\frac{D_+(a)}{a}\right)_{\chi''}\\&\times\int_\chi^{\chi_H}{\rm d}\chi_2'd_{\rm j}(\chi_2')\left(\frac{{\rm d}D_+(a)}{{\rm d}\eta}\right)_{\chi_2'}(\ell^2+(k'\chi_2')^2)^2P_{\Phi\delta}\left(k';0\right)P_\Phi\left(\frac{\sqrt{\ell^2+(k'\chi_2')^2}}{\chi};0\right)j_0'(k'|\chi_2'-\chi''|).\end{aligned} \tag{A14}$$

A3 Redshift space distortions cross-correlations with gravitomagnetic effect

The gravitomagnetic field is sourced by the momentum density, equation (31), and therefore by potentials and derivatives of the density field. We expect to find a correlation between its correction and the redshift distortions that include angular derivatives of the same potential (18).

For the Sachs–Wolfe effect we find,

$$C_{\rm ij}^{\rm SG}(\ell)=\frac{-2}{c^6}\int_0^{\chi_H}\frac{{\rm d}\chi}{\chi^2}\int\frac{{\rm d}k'}{2\pi^2}M_{\rm ij}^{\rm SG}(k',\ell;\chi), \tag{A15}$$

with,

$$\begin{aligned}M_{\rm ij}^{\rm SG}(k',\ell;\chi)=&\int_\chi^{\chi_H}{\rm d}\chi'g_{\rm i}(\chi,\chi')\frac{\rm d}{{\rm d}\eta}\left(\frac{D_+(a)}{a}\right)_\chi\int_\chi^{\chi_H}{\rm d}\chi''\left(\frac{D_+(a)}{a}\right)_{\chi''}d_{\rm j}(\chi'')k'(\ell^2+(k'\chi)^2)\\&\times P_{\delta\Phi}(k';0)P_{\delta\Phi}\left(\frac{\sqrt{l^2+(k'\chi)^2}}{\chi};\chi\right)j_0'(k'|\chi-\chi''|).\end{aligned} \tag{A16}$$

On the other hand, the correlation with the integrated Sachs–Wolfe effect contributes with,

$$C^{\rm IG}=\frac{-4}{c^7}\int_0^{\chi_H}\frac{{\rm d}\chi}{\chi^2}\int\frac{{\rm d}k'}{2\pi^2}M_{\rm ij}^{\rm IG}(k',\ell;\chi), \tag{A17}$$

where,

$$\begin{aligned}M_{\rm ij}^{\rm IG}(k',\ell;\chi)=&\left(\frac{{\rm d}D_+(a)}{{\rm d}\eta}\right)_\chi\int_\chi^{\chi_H}{\rm d}\chi_1'g_{\rm i}(\chi,\chi_1')\int_\chi^{\chi_H}{\rm d}\chi_2'{\rm d}_{\rm j}(\chi_2')\\&\times\int_0^{\chi_2'}d\chi''\frac{\rm d}{{\rm d}\eta}\left(\frac{D_+(a)}{a}\right)_{\chi''}k'P_{\delta\Phi}(k';0)P_\Phi\left(\frac{\sqrt{\ell^2+(k'\chi)^2}}{\chi};\chi\right)(\ell^2+(k'\chi)^2)j_0'(k'|\chi-\chi''|).\end{aligned} \tag{A18}$$

Finally, peculiar motions add,

$$C_{\rm ij}^{\rm VG}(\ell)=\frac{2}{c^5}\int_0^{\chi_H}\frac{{\rm d}\chi}{\chi^2}\int\frac{{\rm d}k'}{2\pi^2}M_{\rm ij}^{\rm VG}(k',\ell;\chi), \tag{A19}$$

with,

$$M_{\rm ij}^{\rm VG}(k',\ell;\chi)=k'^2\left(\frac{{\rm d}D_+(a)}{{\rm d}\eta}\right)_\chi^2d_{\rm i}(\chi)\int_\chi^{\chi_H}{\rm d}\chi_1'g_{\rm i}(\chi,\chi_1')\int_\chi^{\chi_H}d\chi''(\ell^2+(k'\chi)^2)j_0''(k'|\chi-\chi''|)P_\Phi(k';0)P_{\delta\Phi}\left(\frac{\sqrt{\ell^2+(k'\chi)^2}}{\chi};\chi\right) \tag{A20}$$

A4 Redshift space distortions with second-order light propagation

In this case, there is a correlation between them since both corrections, (18) and (24), contain angular derivatives of the potential. The correlation with peculiar velocities,

$$C_{\rm ij}^{\rm VP}(\ell)=\frac{2\ell^2}{c^6}\int_0^{\chi_H}\frac{{\rm d}\chi}{\chi^2}\int\frac{{\rm d}k'}{2\pi^2}k'M_{\rm ij}^{\rm VP}(k',\ell;\chi). \tag{A21}$$

with

$$M_{\rm ij}^{\rm VP}(k',\ell;\chi)=\left(\frac{D_+(a)}{a}\right)_\chi\int_\chi^{\chi_H}{\rm d}\chi' g_{\rm i}(\chi,\chi')\times\int_\chi^{\chi_H}{\rm d}\chi''\left(\frac{{\rm d}D_+(a)}{{\rm d}\eta}\right)_{\chi''}d_{\rm j}(\chi'')(\ell^2+(k'\chi'')^2)$$
$$P_{\Phi\delta}\left(k';0\right)P_\Phi\left(\frac{\sqrt{\ell^2+(k'\chi'')^2}}{\chi};\chi\right)j_0'(k'|\chi-\chi''|), \tag{A22}$$

whereas with the Sachs–Wolfe effect,

$$C_{\rm ij}^{\rm SP}(\ell)=\frac{2\ell^2}{c^7}\int_0^{\chi_H}\frac{{\rm d}\chi}{\chi^4}\int\frac{{\rm d}^2\ell'}{(2\pi)^2}(\ell')^2M_{\rm ij}^{\rm SP}(\ell',|\boldsymbol{\ell}-\boldsymbol{\ell}'|;\chi) \tag{A23}$$

$$M_{\rm ij}^{\rm SP}(\ell,\ell';\chi)=\int_\chi^{\chi_H}{\rm d}\chi' g_{\rm i}(\chi,\chi')d_{\rm j}(\chi)P_\Phi\left(\frac{\ell}{\chi};\chi\right)P_\Phi\left(\frac{\ell'}{\chi};\chi\right) \tag{A24}$$

and finally with the integrated Sachs–Wolfe effect,

$$C^{\rm IP}=-\frac{4\ell^2}{c^8}\int_0^{\chi_H}\frac{{\rm d}\chi}{\chi^4}\int\frac{{\rm d}^2\ell'}{(2\pi)^2}(\ell')^2M_{\rm ij}^{\rm IP}(\ell',|\boldsymbol{\ell}-\boldsymbol{\ell}'|;\chi) \tag{A25}$$

with,

$$M_{\rm ij}^{\rm IP}(\ell,\ell';\chi)=\int_\chi^{\chi_H}{\rm d}\chi' g_{\rm i}(\chi,\chi')\int_\chi^{\chi_H}{\rm d}\chi'' d_{\rm j}(\chi'')P_\Phi\left(\frac{\ell}{\chi};\chi\right)P_\Phi\left(\frac{\ell'}{\chi};\chi\right). \tag{A26}$$

A5 Second-order light propagation with temporal Born

Again, the angular derivatives of the potential in equations (18) and (27) produce the following non-zero correlation,

$$C^{\rm PB}=\frac{4\ell^2}{c^9}\int_0^{\chi_H}\frac{{\rm d}\chi}{\chi^4}\int\frac{{\rm d}^2\ell'}{(2\pi)^2}(\ell')^2M_{\rm ij}^{\rm PB}(\ell',|\boldsymbol{\ell}-\boldsymbol{\ell}'|;\chi) \tag{A27}$$

with,

$$M_{\rm ij}^{\rm PB}(\ell,\ell';\chi)=\frac{\rm d}{{\rm d}\eta}\left(\frac{D_+(a)}{a}\right)_\chi\left(\frac{D_+(a)}{a}\right)_\chi\int_\chi^{\chi_H}{\rm d}\chi' g_{\rm i}(\chi,\chi')\int_\chi^{\chi_H}{\rm d}\chi'' g_{\rm j}(\chi,\chi'')P_\Phi\left(\frac{\ell}{\chi};\chi\right)P_\Phi\left(\frac{\ell'}{\chi};0\right) \tag{A28}$$

A6 Second-order light propagation with gravitomagnetic effect

This case is special, since both corrections are evaluated at the same comoving distance χ. While the second-order light propagation correction (24) is always positive due to the gravitational potential being squared, the density currents that source the gravitomagnetic effect (31) can be positive or negative depending on the neighbouring structure. In a homogeneous universe, we find on average as many negatives as positives currents and therefore the total average vanishes. This is exactly what we obtain numerically, and therefore the correlation between both corrections vanishes,

$$C_{\rm ij}^{\rm PG}=0. \tag{A29}$$

A7 Gravitomagnetic effect with temporal Born correction

For these two, the angular derivatives produce as well the following non-zero contribution,

$$C_{\rm ij}^{\rm BG}(\ell)=\frac{4}{c^8}\int_0^{\chi_H}\frac{{\rm d}\chi}{\chi^2}\int_0^\infty\frac{{\rm d}k'}{2\pi^2}M_{\rm ij}^{\rm BG}(k',\ell;\chi), \tag{A30}$$

with,

$$M_{\rm ij}^{\rm BG}(k',\ell;\chi)=\left(\frac{{\rm d}D_+(a)}{{\rm d}\eta}\right)_\chi\left(\frac{D_+(a)}{a}\right)_\chi\frac{\rm d}{{\rm d}\eta}\left(\frac{D_+(a)}{a}\right)_\chi k'\int_\chi^{\chi_H}{\rm d}\chi_1' g_{\rm i}(\chi,\chi_1')\int_\chi^{\chi_H}{\rm d}\chi_2' g_{\rm j}(\chi,\chi_2')$$
$$\times\int_\chi^{\chi_2'}{\rm d}\chi''\left(\frac{D_+(a)}{a}\right)_{\chi''}(\ell^2+(k'\chi)^2)j_0'(k'|\chi-\chi''|)P_\Phi(k';0)P_{\delta\Phi}\left(\frac{\sqrt{\ell^2+(k'\chi)^2}}{\chi};0\right). \tag{A31}$$

This paper has been typeset from a TEX/LATEX file prepared by the author.